

# OBSERVATIONAL CONSTRAINTS ON THE GENERALIZED CHAPLYGIN GAS

SERGIO DEL CAMPO

*Instituto de Física, Pontificia Universidad de Católica de Valparaíso, Casilla 4950  
Valparaíso , Chile  
sdelcamp@ucv.cl*

J.R.VILLANUEVA

*Instituto de Física, Pontificia Universidad de Católica de Valparaíso, Casilla 4950  
Valparaíso , Chile  
jose.villanueva.l@mail.ucv.cl*

In this paper we study a quintessence cosmological model in which the dark energy component is considered to be the Generalized Chaplygin Gas and the curvature of the three-geometry is taken into account. Two parameters characterize this sort of fluid, the  $\nu$  and the  $\alpha$  parameters. We use different astronomical data for restricting these parameters. It is shown that the constraint  $\nu \lesssim \alpha$  agrees enough well with the astronomical observations.

*Keywords:* Dark Energy; exotic fluid.

## 1. Introduction

Current measurements of redshift and luminosity-distance relations of Type Ia Supernovae (SNe) indicate that the expansion of the Universe presents an accelerated phase<sup>1,2</sup>. In fact, the astronomical measurements showed that Type Ia SNe at a redshift of  $z \sim 0.5$  were systematically fainter which could be attributed to an acceleration of the universe caused by a non-zero vacuum energy density. This gives as a result that the pressure and the energy density of the universe should violate the strong energy condition,  $\rho_X + 3p_X > 0$ , where  $\rho_X$  and  $p_X$  are energy density and pressure of some matter denominated dark energy, respectively. A direct consequence of this, it is that the pressure must be negative. However, although fundamental for our understanding of the evolution of the universe, its nature remains a completely open question nowadays.

Various models of dark energy have been proposed so far. Perhaps, the most traditional candidate to be considered is a non-vanishing cosmological constant<sup>3,4</sup>. Other possibilities are quintessence<sup>5,6</sup>, k-essence<sup>7,8,9</sup>, phantom field<sup>10,11,12</sup>, holographic dark energy<sup>13,14</sup>, etc. (see ref. 15 for model-independent description of the properties of the dark energy and ref. 16 for possible alternatives).

One of the possible candidate for dark energy that would like to consider here

is the so-called Chaplygin gas (CG) <sup>17</sup>. This is a fluid described by a quite unusual equation of state, whose characteristic is that it behaves as a pressureless fluid at the early stages of the evolution of the universe and as a cosmological constant at late times. Actually, in ref. 18, it was recognized its relevance to the detected cosmic acceleration. They found that the CG model exhibits excellent agreement with observations. From this time, the cosmological implications of the CG model have been intensively investigated in the literature <sup>19,20,21,22</sup>. Subsequently, it was noticed that this model can be generalized, which now it is called the generalized Chaplygin gas (GCG). This GCG model was introduced in ref. 18 and elaborated in ref. 23. After these works, the cosmological implications of the GCG model have been intensively investigated in the literature <sup>24,25,26,27,28,29,30,31,32</sup>. There are claims that it does not pass the test connected with structure formation because of predicted but not observed strong oscillations of the matter power spectrum <sup>33</sup>. It should be mentioned, however, the oscillations in the Chaplygin gas component do not necessarily imply corresponding oscillations in the observed baryonic power spectrum <sup>34</sup>. This is a topic that requires much more studies. It was realized that these kind of models have a clearly stated connection with high-dimension theories <sup>35</sup>. Here, the GCG appears as an effective fluid associated with d-branes. Also, at the fundamental level, it could be derived from the Born-Infeld action <sup>36</sup>.

On the other hand, today we do not know precisely the geometry of the universe, since we do not know the exact amount of matter present in the Universe. Various tests of cosmological models, including spacetime geometry, galaxy peculiar velocities, structure formation and very early universe descriptions (related to the Guths inflationary universe model <sup>37</sup>) support a flat universe scenario. Specifically, by using the five-year Wilkinson Microwave Anisotropy Probe (WMAP) data combined with measurements of Type Ia supernovae (SN) and Baryon Acoustic Oscillations (BAO) in the galaxy distribution, was reported the following value for the total matter density parameter,  $\Omega_T$ , at the 68% CL uncertainties,  $\Omega_T = 1.02 \pm 0.02$  <sup>38</sup>.

In this respects we wish to study universe models that have curvature and are composed by two matter components. One of these components is the usual nonrelativistic dark matter (dust); the other component corresponds to dark energy which is supposed to be a sort of quintessence-type matter, described by a Chaplygin gas-type, or more specifically the GCG.

We should mention that in what concern with the Bayesian analysis the cosmological constant is favored over GCG <sup>39,40,41</sup>. However, in ref. <sup>42</sup>, it was shown that the GCG models, proposed as candidates of the unified dark matter-dark energy (UDME), are tested with the look-back time (LT) redshift data. They found that the LT data only give a very weak constraint on the parameters. But, when they combine the LT redshift data with the baryonic acoustic oscillation peak the GCG appears as a viable candidate for dark energy. On the other hand, the GCG model has been constrained with the integrated Sachs-Wolf effect. Recently, a gauge-invariant analysis of the baryonic matter power spectrum for GCG cosmologies was

shown to be compatible with the data <sup>43,32,44</sup>. This result seems to strengthen the role of Chaplygin gas type models as competitive candidates for the dark sector.

Our paper is organized as follow: In section II we present the main characteristic properties and we introduce some definition related to the GCG. In section III we study the kinematics of our model. Here, we take quantities such that the modulus distance, luminosity distance, angular size, among others. In section IV we proceed to describe the so-called shift parameter which is related to the position of the first acoustic peak in the power spectrum of the temperature anisotropies of the cosmic microwave background (CMB) anisotropies. We give our conclusions in Section V.

## 2. The Generalized Chaplygin Gas (GCG)

Let us start by considering the equation of state (EOS) corresponding to the GCG

$$p_{gcg} = -\nu \frac{\Xi}{\rho_{gcg}^\alpha}. \quad (1)$$

Here,  $p_{gcg}$  and  $\rho_{gcg}$  are the pressure and the energy density related to the GCG, respectively.  $\nu$  is the square of the actual speed of sound in the GCG and  $\alpha$  is the GCG index.  $\Xi$  is a function of  $\alpha$  and  $\rho_{gcg}^{(0)}$  (the present value of the energy density of the GCG), and it is given by

$$\Xi \equiv \Xi(\rho_{gcg}^{(0)} | \alpha) = \frac{1}{\alpha} \left( \rho_{gcg}^{(0)} \right)^{1+\alpha}. \quad (2)$$

The dimensionless energy density related to the GCG  $f_{gcg}(z; \nu, \alpha) \equiv \rho_{gcg}(z; \nu, \alpha) / \rho_{gcg}^{(0)}$  becomes given as a function of the red shift,  $z$ , and the parameters  $\alpha$  and  $\nu$  as follows

$$f_{gcg}(z; \nu, \alpha) = \left[ \frac{\nu}{\alpha} + \left( 1 - \frac{\nu}{\alpha} \right) (1+z)^{3(1+\alpha)} \right]^{\frac{1}{1+\alpha}}. \quad (3)$$

Here, we have considering a Friedmann-Robertson-Walker (FRW) metric, and we have used the energy conservation equation:  $\frac{d\rho_{gcg}}{dt} + 3H(\rho_{gcg} + p_{gcg}) = 0$ , where  $H$  represents the Hubble factor. Note that if  $\alpha = \nu$ , we get that  $f_{gcg}(z, \alpha) = 1$  (the same happen for  $z = 0$ ), which means that the energy density related to the GCG corresponds to a cosmological constant.

In Fig.1 we plot  $f_{gcg}(z; \nu, \alpha)$  as a function of the red shift,  $z$ . Note that this function is highly sensitive to the difference between the values of  $\alpha$  and  $\nu$ .

The derivative of the function  $f_{gcg}(z; \nu, \alpha)$  with respect to the redshift,  $z$ , becomes given by

$$\frac{df_{gcg}(z; \nu, \alpha)}{dz} \equiv f'_{gcg}(z; \nu, \alpha) = 3 \left( 1 - \frac{\nu}{\alpha} \right) \frac{(1+z)^{3\alpha+2}}{f^\alpha(z; \nu, \alpha)}.$$

Note that the sign of this function depends on the values that the constants  $\nu$  and  $\alpha$  could take. For  $\nu \geq \alpha$  we have that  $f'_{gcg}(z; \nu, \alpha) \leq 0$ . We need to have that

4 *Sergio del Campo and José Villanueva*

the function  $f_{gcg}(z; \nu, \alpha)$  to be greater than zero, since it corresponds to an energy density in an expanding universe. Thus, we expect that the case  $\nu < \alpha$  be relevant for our study.

We can write the EOS related to the GCG in the barotropic form as follows

$$p_{gcg} = \omega_{gcg} \rho_{gcg}, \quad (4)$$

where the equation of state parameter,  $\omega_{gcg}(z)$ , becomes given by

$$\omega_{gcg}(z) = -\frac{\nu/\alpha}{\frac{\nu}{\alpha} + \left(1 - \frac{\nu}{\alpha}\right)(1+z)^{3(1+\alpha)}}. \quad (5)$$

Of course, for  $\nu = \alpha = 0$  we get  $\omega_{gcg} = -1$ , corresponding to the cosmological constant case. In Fig.2 we have plotted the EOS parameter,  $\omega(z; \nu, \alpha)$ , as a function of the red shift,  $z$ . Note that for  $z_c = \left(\frac{1}{1-\alpha/\nu}\right)^{\frac{1}{3(1+\alpha)}} - 1$ , with  $\alpha < \nu$ , the EOS parameter,  $\omega(z_c; \nu, \alpha)$ , goes to minus (plus) infinity, i.e.  $\omega(z_c; \nu, \alpha) \rightarrow \mp\infty$ . The minus (plus) sign corresponds to the  $z < z_c$  ( $z > z_c$ ) branch. These situations are represented in Fig.2 by the blue lines. For an accelerating phase of the universe we need to take into account the  $z < z_c$  branch only, since it gives the right negative sign for the EOS parameter. For  $\alpha > \nu$ , the EOS parameter always is negative, i.e.  $-\frac{\nu}{\alpha} \leq \omega_{gcg} < 0$ . Summarizing, we can see from the latter equation that for  $\nu > \alpha$  we have  $-1 < -\nu/\alpha \leq \omega_{gcg} < 0$  and for  $\nu < \alpha$  we find that  $-1 > -\nu/\alpha \geq \omega_{gcg} > -\infty$ .

A Taylor expansion of the EOS parameter,  $\omega_{gcg}(z)$ , around  $z = 0$  becomes

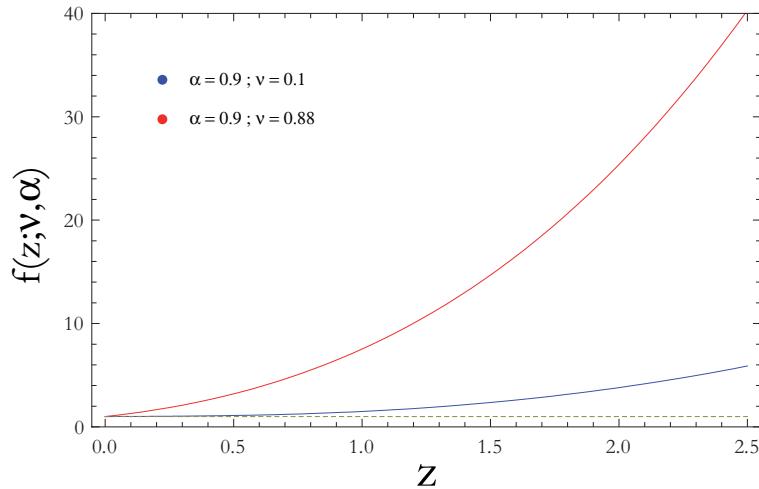


Fig. 1. Plot of the function  $f_{gcg}(z; \nu, \alpha)$  as a function of the red shift,  $z$  for the cases  $\alpha > \nu$  ( $\alpha = 0.9$ ;  $\nu = 0.1$ , blue line) and  $\alpha \approx \nu$  ( $\alpha = 0.9$ ;  $\nu = 0.88$ , red line). These two cases are compared with that corresponding to the cosmological constant,  $\Lambda$ , case (dashed line).

$$\omega_{gcg}(z) = -\beta + 3\beta(1-\beta)(1+\alpha)z - 3\beta(1-\beta)(1+\alpha)[3(1-2\beta)(1+\alpha) + 1]z^2 + O(z^3), \quad (6)$$

where  $\beta = \frac{\nu}{\alpha}$ .

In a spatially flat universe, the combination of WMAP and the Supernova Legacy Survey (SNLS) data leads to a significant constraint on the equation of state parameter for the dark energy  $w(0) = -0.967^{+0.073}_{-0.072}$  <sup>45</sup>. This constraint restricts the value of the ratio  $\frac{\nu}{\alpha}$ . The value of this ratio used above, (see Fig. 1), lies inside the observational astronomical range of the parameter  $\omega(0)$ . The case in which the EOS parameter is a linear function of the redshift was studied in <sup>46,47</sup>. This, it is a good parametrization at a low redshift.

Phenomenological models of a specific time dependent parametrization of the EOS, together with a constant speed of sound have being described in the literature. A simple example is the parametrization expressed by the EOS <sup>48,49</sup>  $\omega(z) = \omega(0) + \frac{d\omega(z)}{dz} \bigg|_0 \frac{z}{(1+z)}$  corresponding to non-interacting dark energy. By matching this parametrization with our expression at low redshift we find that the parameter  $\frac{d\omega(z)}{dz} \bigg|_0$  and  $3\beta(1-\beta)(1+\alpha)$  coincides. The determination of the dynamical character of the EOS parameter,  $\omega(z)$ , becomes important in future experiments. This relevance has been notice by the The Dark Energy Task Force (DETF) <sup>50</sup>. The coming decade will be an exciting period for dark energy research.

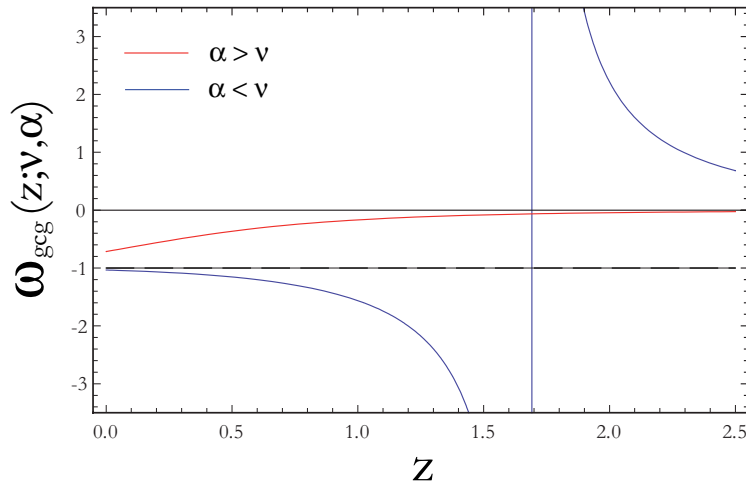


Fig. 2. Plot of the EOS parameter,  $\omega(z; \nu, \alpha)$ , as a function of the red shift,  $z$ . This function for  $\nu < \beta$  lies in the range between  $-\nu/\beta$  (for  $z = 0$ ) and 0 (for  $z \rightarrow \infty$ ). For  $\nu = \beta$  this parameter gets the value  $-1$ , and for  $\nu > \beta$  this parameter present two branches (one positive and the other negative). It becomes  $\omega_{gcg} \rightarrow \mp\infty$  at some specific value of the red shift,  $z = z_c$ .

### 3. KINEMATICS OF THE MODEL

In order to describe some important distances we introduce the dimensionless Hubble function,  $E(z) = \frac{H(z)}{H_0}$ , reads as

$$E^2(z; \nu, \alpha) = \Omega_{cdm}^{(0)}(1+z)^3 + \Omega_k^{(0)}(1+z)^2 + \Omega_{gcg}^{(0)}f_{gcg}(z; \nu, \alpha), \quad (7)$$

where  $\Omega_k^{(0)} = -k/H_0^2$ , and  $\Omega_{cdm}^{(0)}$  and  $\Omega_k^{(0)}$  represent the present cold dark matter and curvature density parameters, respectively. Here, the parameter  $k$  takes the values  $-1$ ,  $0$  or  $+1$ , for open, flat or closed geometries, respectively.  $H_0 \equiv H(0) = 100 h \text{ km s}^{-1} \text{ Mpc}^{-1}$  is the current value of the Hubble parameter. The  $E(z; \nu, \alpha)$  quantity depends on the values of the parameters  $\alpha$  and  $\nu$ , apart of the actual values of the density parameters,  $\Omega_k^{(0)}$ ,  $\Omega_{cdm}^{(0)}$  and  $\Omega_{gcg}^{(0)}$ . Note that these latter parameters satisfy the constraint  $\Omega_k^{(0)} + \Omega_{cdm}^{(0)} + \Omega_{gcg}^{(0)} = 1$ . On the other hand, astronomical measurements will constraint the  $\alpha$  and  $\nu$  parameters, as we will see.

In FIG.3 we have taken  $\Omega_{gcg}^{(0)} = 0.725$  and  $\Omega_{cdm}^{(0)} = 0.275$  with  $\Omega_k^{(0)} = 0$  for the theoretical curves, and we have introduced the observational values for the Hubble parameter from Ref. 51. The curves were plotted for both regimes,  $\alpha \gtrsim \nu$  ( $\alpha = 0.9$  and  $\nu = 0.88$ ) and  $\alpha \gg \nu$  ( $\alpha = 0.9$  and  $\nu = 0.1$ ). In order to compare these curves with the standard model we have included the  $\Lambda$ CDM model, also. Note that the curve with  $\alpha \gtrsim \nu$  is closed to the observational data than that curve corresponding to  $\alpha \gg \nu$ . Thus, when curvature is present into the cosmological model, the curve with  $\alpha \gtrsim \nu$  competes with the standard cosmology (the  $\Lambda$ CDM model), in this respect. Note also that no difference between the  $\Lambda$ CDM model and that model were a GCG is included together with the curvature is found for low redshift.

#### 3.1. Luminosity distance - redshift

One of the more important observable magnitudes that we will consider here will be luminous distance,  $d_L$ . This is defined as the ratio of the emitted energy per unit time,  $\mathcal{L}$ , and the energy received per unit time  $\mathcal{F}$  <sup>52</sup>

$$d_L = \frac{\mathcal{L}}{4\pi\mathcal{F}}. \quad (8)$$

In this way, the luminosity distance can be written as

$$d_L(z; \nu, \alpha) = H_0^{-1}(1+z)y(z; \nu, \alpha), \quad (9)$$

where the function  $y(z; \nu, \alpha)$  becomes given by

$$y(z; \nu, \alpha) = \frac{1}{\sqrt{|\Omega_k^{(0)}|}} S_k \left\{ \sqrt{|\Omega_k^{(0)}|} \int_0^z \frac{dz'}{E(z'; \nu, \alpha)} \right\}, \quad (10)$$

and  $S_k(x)$  takes the following expression for the different values of the parameter  $k$ ,

$$S_k(x) \begin{cases} \sin(x), & k = +1; \\ x, & k = 0; \\ \sinh(x), & k = -1. \end{cases} \quad (11)$$

By using the samples of 192 supernova standard candles, 30 radio galaxy and 38 cluster standard rulers, presented in ref. 53, we check our model described by Eq. (10). This check is done under the assumption that the curvature density parameter,  $\Omega_k^{(0)}$  takes the value  $\Omega_k^{(0)} = 0.0045$  and the other parameters are  $\Omega_{gcg}^{(0)} = 0.7165$  and  $\Omega_{cdm}^{(0)} = 0.2790$ . Fig.4 shows some curves related to our model. It is clear that the range of parameters for the GCG, as before, it is near to the limit  $\alpha \gtrsim \nu$ , better that the limit  $\alpha \gg \nu$ . Nevertheless, we cannot discriminate with facility when we compare our curves (for the  $\alpha \gtrsim \nu$  case) with that corresponding to the  $\Lambda$ CDM model. However, this comparison becomes indistinguishable for small redshift, i.e.  $z \lesssim 0.7$ .

One interesting quantity related to the luminosity distance,  $d_L$ , is the distance modulus,  $\mu$ , which is defined as <sup>54</sup>

$$\mu = 5 \log_{10}[d_L/(1\text{Mpc})] + 25. \quad (12)$$

In Fig.5 we have plotted  $\mu$  as a function of the redshifts,  $z$ . The values for the

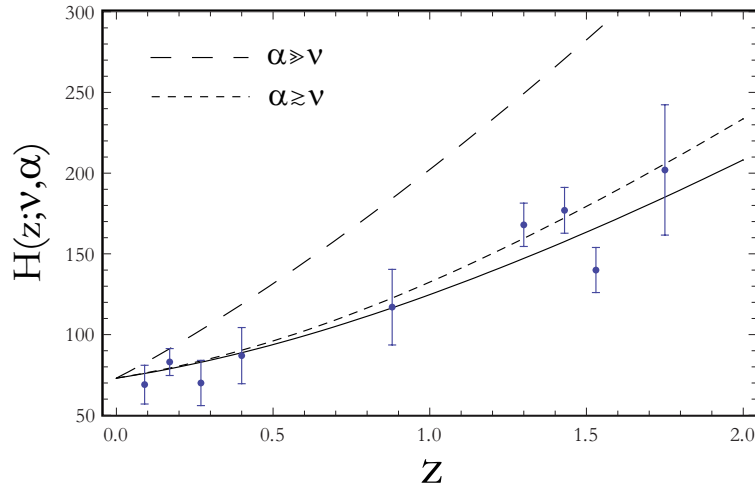


Fig. 3. Plot of the Hubble parameter,  $H(z; \nu, \alpha)$ , as a function of the redshift,  $z$ . Here, we have introduced the observational values for the Hubble's parameter (see ref. 16). The analytical curves were determined by using  $H_0 = 73[\text{Mpc}^{-1}\text{Km/s}]$  for the present value of the Hubble's parameter and we have taken  $\Omega_{gcg}^{(0)} = 0.725$  and  $\Omega_{cdm}^{(0)} = 0.275$  for a flat geometry. The two GCG curves (small and large dashed) were plotted by taking  $\alpha = 0.9 \gg \nu = 0.1$  and  $\alpha = 0.9 \gtrsim \nu = 0.88$ . The solid line represents the  $\Lambda$ CDM model.

different GCG parameters are the two set:  $\alpha = 0.9$  and  $\nu = 0.88$ , and  $\alpha = 0.9$  and  $\nu = 0.01$ . In each case we have considered that  $\Omega_{cdm}^{(0)} = 0.279$ ,  $\Omega_{gcg}^{(0)} = 0.7255$  and  $\Omega_k^{(0)} = -0.0045$ . Also, we have included in this plot the  $\Lambda$ CDM model, with  $\Omega_{\Lambda}^{(0)} = \Omega_{gcg}^{(0)} = 0.7255$ . The data included in this graph were taken from ref. 55. Note that the case for  $\nu \lesssim \alpha$  becomes practically indistinguishable from that corresponding to the  $\Lambda$ CDM model.

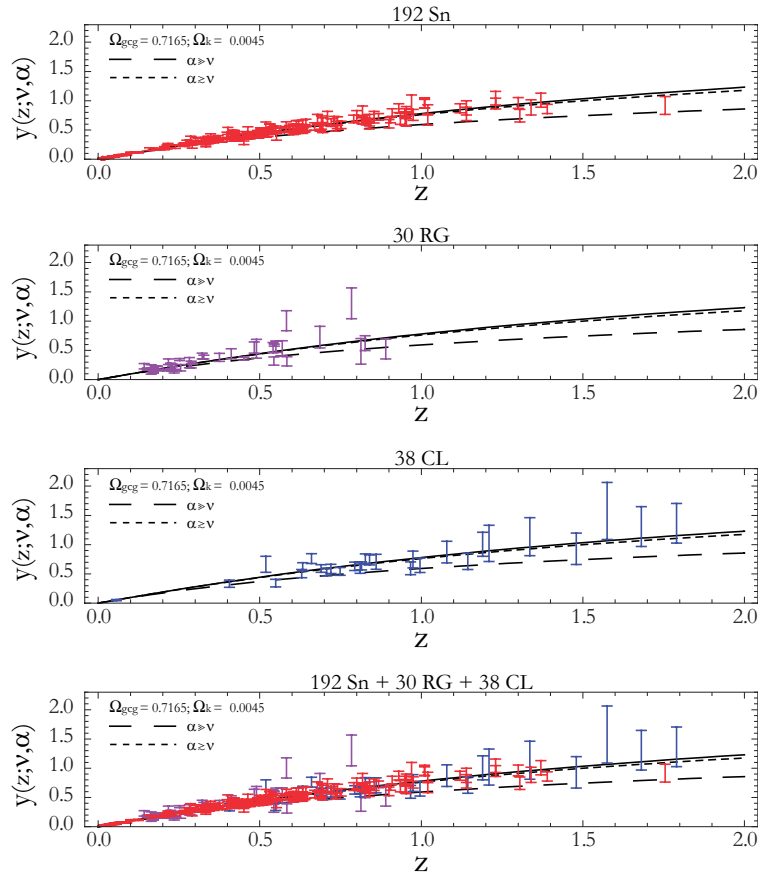


Fig. 4. Plots of the theoretical curves for  $y(z; \nu, \alpha)$  as a function of the redshift,  $z$  for two different regimes:  $\nu = 0.1 \ll \alpha = 0.9$  and  $\nu = 0.88 \lesssim \alpha = 0.9$ . These curves are compared with astronomical data extracted from Daly *et al* 2007; Left top: 192 Supernovas (Sn); Right top: 30 Radio Galaxies (RG); Left down: 38 Galaxy Clusters (CL); Right down: 192 Sn + 30 RG + 38 CL. Here, we have taken the values  $\Omega_k^{(0)} = 0.0045$ ,  $\Omega_{gcg}^{(0)} = 0.7165$  and  $\Omega_{cdm}^{(0)} = 0.2790$ .



### 3.2. Angular size - redshift

The angular size,  $\Theta$ , is defined as the ratio of an objects physical transverse size,  $l$ , to the angular diameter distance,  $d_A$ . This latter distance is related to the luminosity distance,  $d_L$  by mean of the relation  $d_A = d_L/(1+z)^2$ . Therefore, we have

$$\Theta(z; \nu, \alpha) \equiv \frac{l}{d_A(z; \nu, \alpha)} = \kappa \frac{1+z}{y(z; \nu, \alpha)}, \quad (13)$$

Here,  $l = l_0 h^{-1}$ , with  $l_0$  the linear size scaling factor and  $\kappa = lH_0/c = 0.432l_0[\text{mas/pc}]$ .

Following our treatment of the comparison of the chaplygin gas with the available data, we use the ref. 56 compilation into 12 bins with 12-13 sources which satisfies the conditions in which the spectral index lies in the range  $-0.38 \leq \eta \leq 0.18$  and a total radio luminosity,  $L$ , which satisfies the constraint,  $Lh^2 \geq 10^{26}[\text{W}/Hz]$ .

This points are showed in FIG.6 together with the curves determined by taking the values  $l_0 = 4.86[\text{pc}]$   $\Omega_{cdm}^{(0)} = 0.2790$ ,  $\Omega_{gcg}^{(0)} = 0.7255$   $\Omega_k^{(0)} = -0.0045$ . Note once again that the case for which  $\alpha \gtrsim \nu$  becomes favored than that the case corresponding to  $\alpha \gg \nu$ . Here, as before we have include the case corresponding to the  $\Lambda$ CDM model specified by a continuous line.

### 3.3. Deceleration, jerk, and snap parameters - redshift

The luminosity distance,  $d_L$ , could be expanded in such a way that the first Taylor coefficients of this expansion are related to the parameters denominated deceleration ( $q$ ), jerk ( $j$ ), and snap ( $s$ ) parameters evaluated at present time. These three parameters are defined in term of the second, third, and fourth derivatives of the scale factor with respect to time, respectively. The expansion of  $d_L$  in term of the redshift,  $z$ , reads<sup>54</sup>

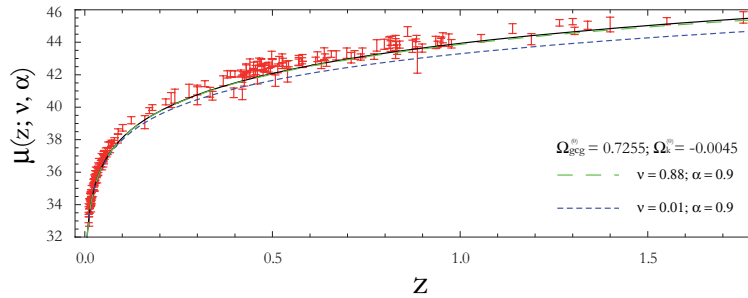


Fig. 5. Graphic representing the magnitude  $\mu(z; \nu, \alpha)$  as a function of the redshifts,  $z$ . Here we have plotted two curves, one for  $\nu \lesssim \alpha$  ( $\alpha = 0.9$  and  $\nu = 0.88$ ) and the other one for  $\nu \ll \alpha$  ( $\nu = 0.01$  and  $\alpha = 0.9$ ). Here, we have taken the values  $\Omega_{gcg}^{(0)} = 0.7255$  and  $\Omega_{cdm}^{(0)} = 0.279$ . Also, we have included in this plot the  $\Lambda$ CDM model, with  $\Omega_{\Lambda}^{(0)} = \Omega_{gcg}^{(0)} = 0.7255$ . The data were taken from Riess *et al* 2004.

$$d_L(z) = \frac{cz}{H_0} \left\{ 1 + \frac{1}{2} [1 - q_0] z - \frac{1}{6} [1 - q_0 - 3q_0^2 + j_0 + \frac{kc^2}{H_0^2 a_0^2}] z^2 + \frac{1}{24} [2 - 2q_0 - 15q_0^2 - 15q_0^3 + 5j_0 + 10q_0 j_0 + s_0 + \frac{kc^2(1+3q_0)}{H_0^2 a_0^2}] z^3 + O(z^4) \right\}. \quad (14)$$

For our model the deceleration parameter,  $q(z; \nu, \alpha)$  becomes given by

$$q(z; \nu, \alpha) = -1 + \frac{(1+z)E'(z; \nu, \alpha)}{E(z; \nu, \alpha)} = \frac{1}{2} \left[ 1 - \frac{3\frac{\nu}{\alpha}\Omega_{gcg}^{(0)}f^{-\alpha}(z; \nu, \alpha) + \Omega_k^{(0)}(1+z)^2}{E^2(z; \nu, \alpha)} \right]. \quad (15)$$

The present value of this parameter becomes

$$q(0; \nu, \alpha) \equiv q_0(\nu, \alpha) = \frac{1}{2} \left[ \Omega_{cdm}^{(0)} - \left( 3\frac{\nu}{\alpha} - 1 \right) \Omega_{gcg}^{(0)} \right]. \quad (16)$$

In order to describe an accelerating universe, we need to satisfy the constraint

$$\frac{\nu}{\alpha} > \frac{1}{3} \left( 1 + \frac{\Omega_{cdm}^{(0)}}{\Omega_{gcg}^{(0)}} \right).$$

Taking the ratio  $\frac{\Omega_{cdm}^{(0)}}{\Omega_{gcg}^{(0)}} \approx \frac{3}{7}$  we get that the  $\nu$  and  $\alpha$  parameters must satisfy the bound  $\frac{\nu}{\alpha} > \frac{10}{21}$ . Note that the values of this ratio that better agree with the astro-

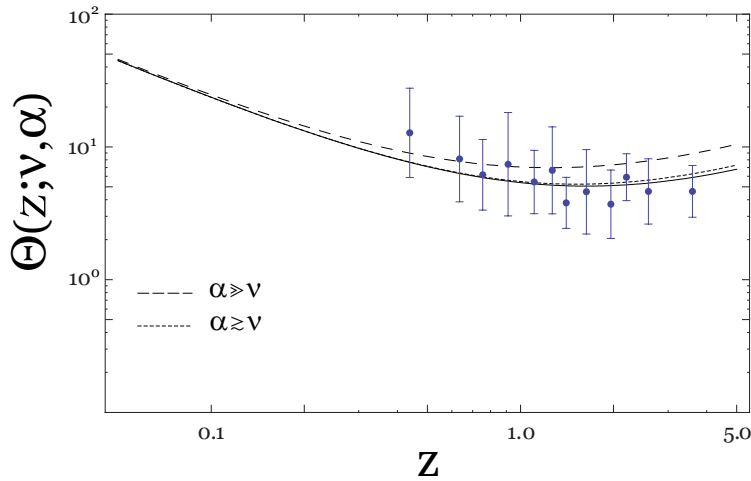


Fig. 6. The angular size,  $\Theta$ , as a function of the redshift,  $z$ . The curves were determined by using the value  $l_0 = 4.86[pc]$  and  $\Omega_{cdm}^{(0)} = 0.2790$ ,  $\Omega_{gcg}^{(0)} = 0.7255$ ,  $\Omega_k^{(0)} = -0.0045$ . The data correspond to 145 sources compiled by Gurvits *et al* 1999.

nomical data described previously satisfy this restriction, since in most of them we have taken  $\nu = 0.88 \lesssim \alpha = 0.9$ .

With respect to the jerk,  $j$ , parameter we have that this becomes given by

$$j(z; \nu, \alpha) = 3q^2(z; \nu, \alpha) + \frac{(1+z)^2 E''(z; \nu, \alpha)}{E(z; \nu, \alpha)}, \quad (17)$$

which, at present time, i.e.  $z = 0$ , it becomes

$$j(0; \nu, \alpha) = 1 - \Omega_k^{(0)} + \frac{9\nu}{2} \left(1 - \frac{\nu}{\alpha}\right) \Omega_{gcg}^{(0)}. \quad (18)$$

In getting this latter expression we have made use of the constraint  $\Omega_{gcg}^{(0)} + \Omega_{cdm}^{(0)} + \Omega_k^{(0)} = 1$ .

This parameter contains information regarding the sound speed of the dark matter component<sup>57</sup>. Also, the use of the jerk formalism infuses the kinematical analysis with a feature in that all  $\Lambda$ CDM models are represented by a single value of the jerk parameter  $j = 1$ . Therefore, the jerk formalism enables us to constrain and facilitates simple tests for departures from the  $\Lambda$ CDM model in the kinematical manner<sup>58</sup>. In this reference (58 and references therein) it is reported the following values for the jerk parameter: from the type Ia supernovae (SNIa) data of the Supernova Legacy Survey project gives  $j = 1.32_{-1.21}^{+1.37}$ , the X-ray galaxy cluster distance measurements gives  $j = 0.51_{-2.00}^{+2.55}$ , the gold SNIa sample data yields a larger value  $j = 2.75_{-1.10}^{+1.22}$ , and the combination of all these three data set gives  $j = 2.16_{-0.75}^{+0.81}$ .

In Fig. 7 we have plotted the jerk,  $j$ , parameter as a function of the redshifts,  $z$ , for the set of parameters ( $\Omega_{gcg}^{(0)} = 0.7255$  and  $\Omega_k^{(0)} = -0.0045$ ), ( $\Omega_{gcg}^{(0)} = 0.721$  and  $\Omega_k^{(0)} = 0$ ) and ( $\Omega_{gcg}^{(0)} = 0.7165$  and  $\Omega_k^{(0)} = 0.0045$ ). These three set of parameters have being plotted for the two cases  $\nu = 0.1 \ll \alpha = 0.9$ . and  $\nu = 0.88 \lesssim \alpha = 0.9$ . Note that for the latter case the jerk function present a maximum which is not present in the other case, when  $\nu \ll \alpha$ . Note also that for  $z \rightarrow \infty$  the jerk parameter goes to the value corresponding to the  $\Lambda$ CDM case. Also, we do not observe much differences for the different type of geometries, since the curves are very similar.

With respect to the snap parameter  $s$  we have that this parameter becomes given by

$$s(z; \nu, \alpha) = 15q^3(z; \nu, \alpha) + 9q^2(z; \nu, \alpha) - 10q(z; \nu, \alpha)j(z; \nu, \alpha) - 3j(z; \nu, \alpha) - \frac{(1+z)^3 E'''(z; \nu, \alpha)}{E(z; \nu, \alpha)}. \quad (19)$$

For a  $\Lambda$ CDM-universe the present expression for the snap parameter becomes

$$s_0 = 1 - \frac{9}{2} \Omega_{cdm},$$

and in our case it becomes at present, i.e.  $z = 0$ ,

$$s(0; \nu, \alpha) = \frac{9\nu\Omega_{gcg}^{(0)}}{4\alpha^2} \left[ 6\alpha^3 + \alpha^2(1 - 18\nu) + 3\nu^2(2 - \Omega_{gcg}^{(0)}) + \alpha(2 + \nu(3\Omega_{gcg}^{(0)} - 5 + 12\nu)) \right] - \frac{7}{2} + \frac{\Omega_k^{(0)}}{4} \left[ 16 + 9\nu\Omega_{gcg}^{(0)} - 2\Omega_k^{(0)} - 3\frac{\nu}{\alpha}(2 + 3\nu)\Omega_{gcg}^{(0)} \right]. \quad (20)$$

Here, we have used the constraint  $\Omega_{gcg}^{(0)} + \Omega_{cdm}^{(0)} + \Omega_k^{(0)} = 1$  also.

In Ref. 59 was reported that the actual value of the snap parameter,  $s_0$ , gets the value  $s_0 = 3.39 \pm 17.13$  for the fit by using the LZ relation<sup>60</sup> and the value  $s_0 = 8.32 \pm 12.16$  for the fit by taking the GGL one<sup>61</sup>.

#### 4. The first Doppler peak of the CMB spectrum and the shift parameter $R$

In this section, we are going to describe the position of the first Doppler peak ( $l_{LS}^{gcg}$ ) for the model studied in the previous section. The scales that are important in determining the shape of the CMB anisotropy spectrum are the sound horizon  $d_s$  at the time of recombination, and the previously introduced angular diameter distance  $d_A^{LS}$  to the last scattering surface. The former defines the physical scales for the Doppler peak structure that depends on the physical matter density ( $\Omega_{cdm}^{(0)}$ ),

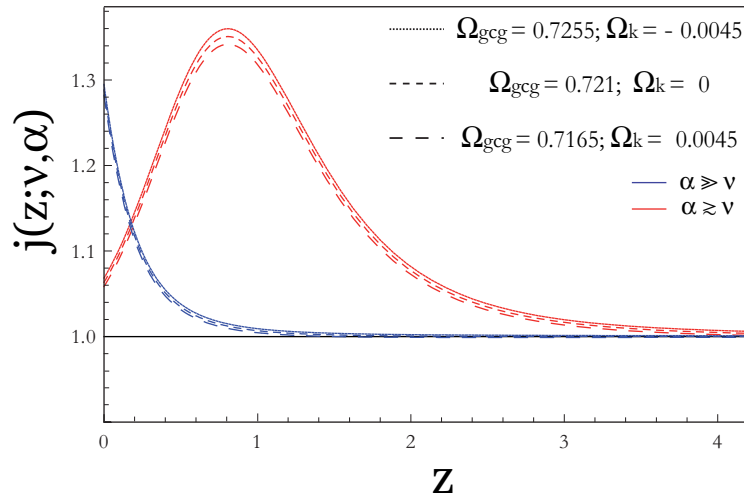


Fig. 7. This plot presents the jerk,  $j$ , parameter as a function of the redshifts,  $z$ . Here, we have taken the following set of parameters: ( $\Omega_{gcg}^{(0)} = 0.7255$  and  $\Omega_k^{(0)} = -0.0045$ ), ( $\Omega_{gcg}^{(0)} = 0.721$  and  $\Omega_k^{(0)} = 0$ ) and ( $\Omega_{gcg}^{(0)} = 0.7165$  and  $\Omega_k^{(0)} = 0.0045$ ). These three set of values have being plotted for the two cases  $\nu = 0.1 \ll \alpha = 0.9$  and  $\nu = 0.88 \lesssim \alpha = 0.9$ .

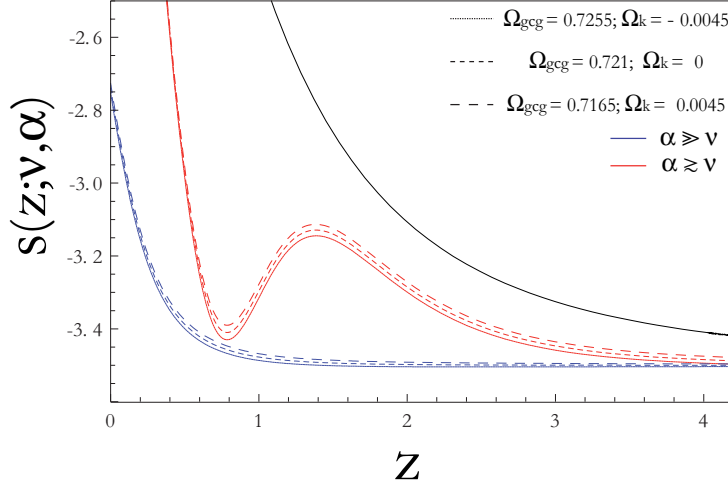


Fig. 8. This plot presents the snap,  $s$ , parameter as a function of the redshifts,  $z$ . Here, as before, we have taken the following set of parameters:  $(\Omega_{gcg}^{(0)} = 0.7255$  and  $\Omega_k^{(0)} = -0.0045)$ ,  $(\Omega_{gcg}^{(0)} = 0.721$  and  $\Omega_k^{(0)} = 0)$  and  $(\Omega_{gcg}^{(0)} = 0.7165$  and  $\Omega_k^{(0)} = 0.0045)$ . These three set of values have being plotted for the two cases  $\nu = 0.1 \ll \alpha = 0.9$  and  $\nu = 0.88 \lesssim \alpha = 0.9$ .

but not on the value of the GCG matter density ( $\Omega_{gcg}^{(0)}$ ) or spatial curvature ( $\Omega_k^{(0)}$ ), since these are dynamically negligible at the time of recombination<sup>62</sup>. The latter depends practically on all of the parameters and is given by

$$d_A^{LS} = \frac{1}{H_0(1+z_{LS})} y(z_{LS}; \nu, \alpha) \quad (21)$$

where  $y(z_{LS}; \nu, \alpha)$  becomes given by (see Eq. 10)

$$y(z_{LS}; \nu, \alpha) = \frac{1}{\sqrt{|\Omega_k^{(0)}|}} S_k \left\{ \sqrt{|\Omega_k^{(0)}|} \int_0^{z_{LS}} \frac{dz'}{E(z'; \nu, \alpha)} \right\}. \quad (22)$$

We may write for the localization of the first Doppler peak

$$l_{LS} \propto \frac{d_A^{LS}}{d_s} \quad (23)$$

where the constant of proportionality depends on both the shape of the primordial power spectrum and the Doppler peak number<sup>63</sup>. Since we are going to keep the  $\Omega_{cdm}^{(0)}$  parameter fixed, we shall take  $l_{LS} \approx d_A^{LS}$ , up to a factor that depends on  $\Omega_{cdm}^{(0)}$  and  $z_{LS}$  only

By using that  $\Omega_k^{(0)} = 1 - \Omega_{cdm}^{(0)} - \Omega_{gcg}^{(0)}$  and following ref. 64 and ref. 65 we can write for the position of the first Doppler peak ( $l_{LS}^{gcg}$ )

$$l_{LS}^{gcg} \sim \Omega_T^{-\eta}, \quad (24)$$

where  $\Omega_T = \Omega_k^{(0)} + \Omega_{cdm}^{(0)} + \Omega_{gcg}^{(0)}$  and

$$\eta = \frac{1}{6} I_1^2 - \frac{1}{2} \frac{I_2}{I_1}, \quad (25)$$

with

$$I_1 = \int_0^1 \frac{dx}{\sqrt{(1 - \Omega_{cdm}^{(0)})x^4 f_{gcg}(1/x - 1; \nu, \alpha) + \Omega_{cdm}^{(0)}x}}, \quad (26)$$

and

$$I_2 = \int_0^1 \frac{x^4 f_{gcg}(1/x - 1; \nu, \alpha) dx}{\sqrt{[(1 - \Omega_{cdm}^{(0)})x^4 f_{gcg}(1/x - 1; \nu, \alpha) + \Omega_{cdm}^{(0)}x]^3}}. \quad (27)$$

where  $x = 1/(1+z)$ .

Note that the model  $\Lambda$ CDM it is obtained when  $f_{gcg} = 1$ , which corresponds to take the values  $\alpha = \nu = 0$  <sup>65</sup>.

In FIG.9 we show the parameter  $\eta$  as a function of the  $\Omega_{cdm}^{(0)}$  parameter. Here, we have taken two different set of values for the gcg parameters,  $\alpha = 0.9; \nu = 0.88$  and  $\alpha = 0.9; \nu = 0.01$ . In order to make a comparison we have included in this plot the  $\Lambda$ CDM model.

One important parameter that describes the dependence of the first Doppler peak position on the different parameters that characterize any model is the shift parameter  $R$ . More specific, it gives the position of the first Doppler peak with respect to its location in a flat reference model with  $\Omega_{cdm}^{(0)} = 1$  <sup>66,67</sup>. This becomes

$$R(\Omega_{cdm}^{(0)}, \Omega_{gcg}^{(0)}; \nu, \alpha) = \sqrt{\frac{\Omega_{cdm}^{(0)}}{|\Omega_k^{(0)}|}} S_k \left[ \sqrt{|\Omega_k^{(0)}|} \int_0^1 \frac{dx}{x^2 E(x; \nu, \alpha)} \right],$$

where  $\Omega_k^{(0)} = 1 - (\Omega_{cdm}^{(0)} + \Omega_{gcg}^{(0)})$ . Note that the initial point is common for the same value of the parameter with different curvature, and the final point is common for the same curvature with different value of the parameters. Note also that if we choose  $\Omega_k^{(0)} = 0$  and  $\alpha = \nu = 0$  ( $f_{gcg}(z; 0, 0) \rightarrow 1$ ) the  $\Lambda$ CDM case is recuperated.

## 5. Conclusions

In this paper we have described and study a cosmological model in which, apart from the usual cold dark matter component, we have included a GCG associated to

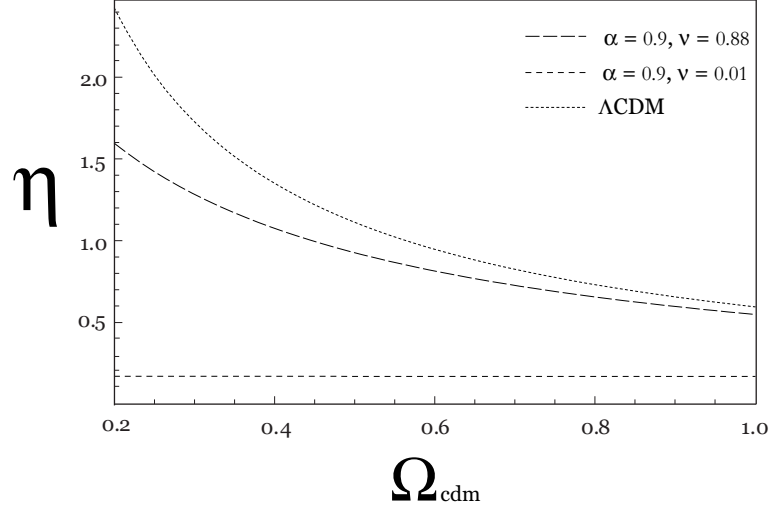


Fig. 9. This graph shows the parameter  $\eta$  as a function of the  $\Omega_{cdm}^{(0)}$  parameter. We have considered two different set of values for the gcg parameters: the set  $(\alpha = 0.9; \nu = 0.88)$  and the set  $(\alpha = 0.9; \nu = 0.01)$ . Here, we have included the  $\Lambda$ CDM case.

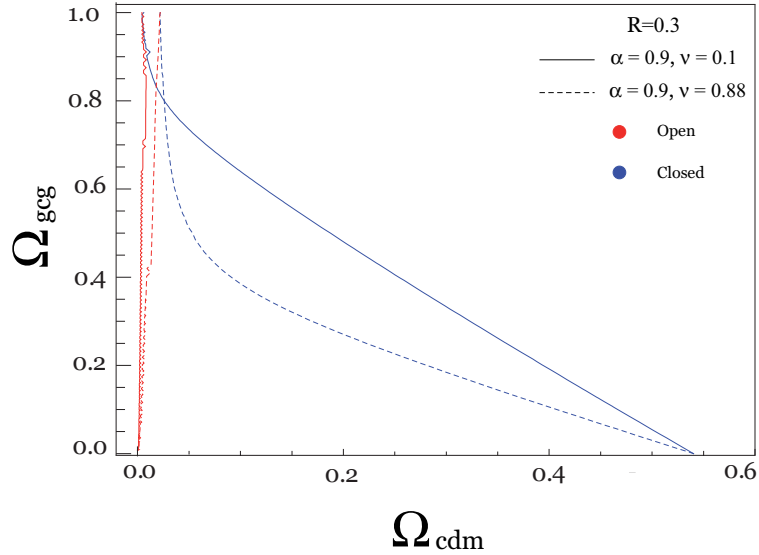


Fig. 10. Contour Plot in the  $\Omega_{gcg}^{(0)} - \Omega_{cdm}^{(0)}$  plane with  $R = 0.3$  for two set of values for the parameters  $\nu$  and  $\alpha$ , i.e.  $\nu = 0.1$  and  $\nu = 0.88$  for  $\alpha = 0.9$ . Here, we have considered positive and negative curvature.

the dark energy component. In this kind of model we have described the properties of the GCG. The characterization of the GCG comes from the determination of the GCG parameters,  $\nu$  and  $\alpha$  related to the velocity of sound of the fluid and the power appearing in the EOS of the GCG, respectively. By taking into account some observational astronomical data, such that the Hubble parameter, the  $y$ -parameter, the angular size and the luminosity distance we were able to restrict these parameters. All of them agree with the condition  $\nu \lesssim \alpha$ . We have also described the deceleration, the jerk and the snap parameters for our model. We expect that with an appropriate data of these parameters will be possible to restrict the parameters of the GCG fluid.

As an applicability of the GCG model described above, we have determined the position of the first Doppler peak together with the shift parameter  $R$ . These cases were compared with that corresponding the  $\Lambda$ CDM model.

We may conclude that, as far as we are concerned with the observed acceleration detected in the universe and the location of the first Doppler peak, we will be able to utilize a GCG model to describe the Universe we live in.

## References

1. A. G. Riess *et al*, *ApJ* **116** (1998) 1009.
2. S. Perlmutter *et al*, *ApJ* **517** (1999) 565.
3. D.N. Spergel *et al*, *ApJ Suppl.* **148** (2003) 175.
4. M. Tegmark *et al*, *Phys. Rev. D* **69** (2004) 103501.
5. R. R. Caldwell, R. Dave and P. J. Steinhardt, *Phys. Rev. Lett.* **80** (1998) 1582.
6. I. Zlatev, L. Wang and P. J. Steinhardt, *Phys. Rev. Lett.* **82** (1998) 896.
7. T. Chiba, T. Okabe and M. Yamaguchi, *Phys. Rev. D* **62** (2000) 023511.
8. C. Armendariz-Picon, V. F. Mukhanov and P. J. Steinhardt, *Phys. Rev. Lett.* **85** (2000) 4438.
9. C. Armendariz-Picon, V. F. Mukhanov and P. J. Steinhardt, *Phys. Rev. D* **63** (2001) 103510.
10. R. R. Caldwell, *Phys. Lett. B* **545** (2002) 23.
11. S. M. Carroll, M. Hoffman and M. Trodden, *Phys. Rev. D* **68** (2003) 023509.
12. S. D. H. Hsu, A. Jenkins and M. B. Wise, *Phys. Lett. B* **597** (2004) 270.
13. X. Zhang, F. Q. Wu, *Phys. Rev. D* **76** (2007) 023502.
14. H. Wei, S. N. Zhang, *Phys. Rev. D* **76** (2007) 063003.
15. R.A. Daly, *A Decade of Dark Energy: 1998 - 2008.*, (2009) [arXiv:astro-ph / 0901.2724].
16. M. Sami, *Dark energy and possible alternatives.*, (2009) [arXiv:hep-th / 0901.0756v1]
17. S. Chaplygin, *Sci. Mem. Moscow Univ. Math* **21** (1904) 1.
18. A. Kamenshchik, U. Moschella and V. Pasquier, *Phys. Lett. B* **511** (2001) 265.
19. A. Dev, D. Jain, and J.S. Alcaniz, *Phys. Rev. D* **67** (2003) 023515.
20. V. Gorini, A. Kamenshchik and U. Moschella, *Phys. Rev. D* **67** (2003) 063509.
21. J.S. Alcaniz and J.A.S. Lima, *AJ* **618** (2005) 16.
22. W. Zimdahl and J. C. Fabris, *Class. Quant. Grav.* **22** (2005) 4311.
23. M.C. Bento, O. Bertolami and A.A. Sen, *Phys. Rev. D* **66** (2002) 043507.
24. L. Amendola, F. Finelli, C. Burigana and D. Carturan, *JCAP* **0307** (2003) 005.
25. M. Makler, S.Q. de Oliveira and I. Waga, *Phys. Lett. B* **555** (2003) 1.
26. F. Perrotta, S. Matarrese and M. Torki, *Phys. Rev. D* **70** (2004) 121304.



27. Z.H. Zhu, *A & A* **423** (2004) 421.
28. O. Bertolami, A.A. Sen, S. Sen and P.T. Silva, *MNRAS* **353** (2004) 329.
29. M.Biesiada, W. Godlowski and M. Szydlowski, *ApJ* **622** (2005) 28.
30. L. Chimento and R. Lazkoz, *Phys. Lett. B* **615** (2005) 146.
31. V. Gorini, A. Kamenshchik, U. Moschella, V. Pasquier and A. Starobinsky, *Phys. Rev. D* **72** (2005) 103518.
32. J.C. Fabris, S.V.B. Goncalves, H.E.S. Velten and W. Zimdahl, *Phys. Rev. D* **78** (2008) 103523.
33. H. B. Sandvik, M. Tegmark, M. Zaldarriaga and I. Waga, *Phys. Rev. D* **69** (2004) 123524.
34. L.M.G. Beça, P.P. Avelino, J.P.M. de Carvalho, and C.J.A.P. Martins, *Phys. Rev. D* **67** (2003) 101301.
35. J.C. Fabris, S.V.B. Goncalves and P.E. De Souza, *Gen. Rel. Grav.* **34** (2002) 2111.
36. M.C. Bento, O. Bertolami and A.A. Sen, *Phys. Lett. B* **575** (2003) 1722003.
37. A. Guth, *Phys. Rev. D* **23** (1981) 347.
38. G. Hinshaw *et al*, *ApJS* **180** (2009) 225.
39. M. Szydlowski, A. Kurek and A. Krawiec, *Phys. Lett. B* **675** (2008) 1.
40. A. Kurek and M Szydlowski, *ApJS* **170** (2007) 377.
41. A. Kurek and M Szydlowski, *Nuovo. Cim.* **122B** (2007) 1359.
42. Z. Li, P. Wu and H. Yu, *Testing the (generalized) Chaplygin gas* (2009) [arXiv:astro-ph / 09083415].
43. V. Gorini, A. Kamenshchik, U. Moschella, O. F. Piatella and A. Starobinsky, *JCAP* **02** (2008) 016.
44. J.C. Fabris, S.V.B. Goncalves, H.E.S. Velten and W. Zimdahl, *Newtonian approach to the matter power spectrum of the Generalized Chaplygin Gas* (2008) [arXiv:astro-ph / 08112367].
45. D.N. Spergel *et al*, *ApJS* **170** (2007) 377.
46. A. R. Cooray and D. Huterer, *ApJ* **513** (1999) L95.
47. E. Di Pietro and J.F. Claeskens, *MNRAS* **341** (2003) 1299.
48. M. Chevallier, D. Polarski, *IJMP D* **10** (2001) 213.
49. E.V. Linder, *Phys. Rev. Lett.* **90** (2003) 091301.
50. A. Albrecht *et al*, *Report of the Dark Energy Task Force.* (2006) [arXiv:astro-ph / 0609591].
51. L. Samushia and B. Ratra, *ApJ* **650** (2006) L5.
52. P.J.E. Peebles and B. Ratra, *Rev. Mod. Phys.* **75** (2003) 559.
53. R.A. Daly *et al*, *Improved Constraints on the Acceleration History of the Universe and the Properties of the Dark Energy.* (2007) [arXiv: astro-ph / 07105345].
54. M. Visser, *Class. Quant. Grav.* **21** (2004) 2603.
55. A. G. Riess *et al*, *ApJ* **607** (2004) 665.
56. L. I. Gurvits, K.I. Kellermann and S. Frey, *A & A* **342** (1999) 378.
57. T. Chiba, T. Nakamura, *Prog. Theor. Phys.* **100** (1998) 1077.
58. D. Rapetti, S. W. Allen, M. A. Amin and R.D. Blandford, *MNRAS* **375** (2007) 1510.
59. S. Capozziello and L. Izzo, *A & A* **490** (2008) 31.
60. E. Liang and B. Zhang, *ApJ* **633** (2005) 611.
61. G. Ghirlanda, G. Ghisellini and D. Lazzati, *ApJ* **616** (2004) 331.
62. G. Efstathiou and J.R. Bond, *MNRAS* **304** (1999) 75.
63. W. Hu and M. White, *ApJ* **471** (1996) 30.
64. S. Weinberg, *Phys. Rev. D* **62** (2000) 127302.
65. S. del Campo, *MNRAS* **339** (2003) 235.
66. R. J. Bond, G. Efstathiou and M. Tegmark, *MNRAS* **291** (1997) L33.

18 *Sergio del Campo and José Villanueva*

67. R. Trotta, *Cosmic Microwave Background Anisotropies: Beyond Standard Parameter*, (2004) [astro-ph/ 0410115]